TBC1D4-S711 Controls Skeletal Muscle Insulin Sensitization After Exercise and Contraction

Rasmus Kjøbsted,[1] Jonas M. Kristensen,[1] Nicolas O. Eskesen,[1] Kohei Kido,[1] Klara Fjorder,[1] Ditte F. Damgaard,[1] Jeppe K. Larsen,[1,2] Nicoline R. Andersen,[1] Jesper B. Birk,[1] Anders Gudiksen,[3] Jonas T. Treebak,[2] Peter Schjerling,[4,5] Henriette Pilegaard,[3] and Jørgen F.P. Wojtaszewski[1]

Diabetes 2023;72:857–871 | https://doi.org/10.2337/db22-0666

The ability of insulin to stimulate glucose uptake in skeletal muscle is important for whole-body glycemic control. Insulin-stimulated skeletal muscle glucose uptake is improved in the period after a single bout of exercise, and accumulating evidence suggests that phosphorylation of TBC1D4 by the protein kinase AMPK is the primary mechanism responsible for this phenomenon. To investigate this, we generated a TBC1D4 knock-in mouse model with a serine-to-alanine point mutation at residue 711 that is phosphorylated in response to both insulin and AMPK activation. Female TBC1D4-S711A mice exhibited normal growth and eating behavior as well as intact whole-body glycemic control on chow and high-fat diets. Moreover, muscle contraction increased glucose uptake, glycogen utilization, and AMPK activity similarly in wild-type and TBC1D4-S711A mice. In contrast, improvements in whole-body and muscle insulin sensitivity after exercise and contractions were only evident in wild-type mice and occurred concomitantly with enhanced phosphorylation of TBC1D4-S711. These results provide genetic evidence to support that TBC1D4-S711 serves as a major point of convergence for AMPK- and insulin-induced signaling that mediates the insulin-sensitizing effect of exercise and contractions on skeletal muscle glucose uptake.

Progressive deterioration of insulin-stimulated skeletal muscle glucose uptake is a hallmark in the etiology of type 2 diabetes (1). Remarkably, a single bout of exercise enhances insulin-stimulated glucose uptake in skeletal muscle from healthy and insulin-resistant subjects (2–5) as well as rodent models (6–8). This effect of exercise may last for up to 48 h (6,9) and highlights the huge potential of exercise to improve insulin-stimulated muscle glucose uptake in diseases characterized by muscle insulin resistance. The insulin-sensitizing effect of acute exercise on muscle glucose uptake seems to rely on elevated muscle perfusion (10) in combination with enhanced GLUT4 translocation (11–13), which occurs independently of changes in proximal insulin signaling (4,5,8,14–16) and protein synthesis (14).

Insulin-stimulated muscle glucose uptake is mediated through an Akt-dependent signaling pathway that involves inhibition of the Rab-GTPase–activating protein TBC1D4 (also known as AS160) by multisite phosphorylation (17,18). This releases intracellular GLUT4 storage vesicles to fuse with the muscle surface membrane, which increases glucose transport capacity (19,20). In mouse skeletal muscle, TBC1D4 is phosphorylated at the serine residue 711 (704 in humans) during insulin stimulation as well as by AMP-activated protein kinase (AMPK) in response to exercise and contraction. However, phosphorylation of TBC1D4-S711 does not seem to be necessary to promote glucose uptake in itself (21).

Several studies in humans and rodents have shown that enhanced insulin-stimulated phosphorylation of TBC1D4 occurs in parallel with improvements in muscle insulin sensitivity after a single bout of exercise and contraction (5,8,15,22–25). We have shown that AMPK is necessary

[1]August Krogh Section for Molecular Physiology, Department of Nutrition, Exercise and Sports, Faculty of Science, University of Copenhagen, Copenhagen, Denmark
[2]Novo Nordisk Foundation Center for Basic Metabolic Research, Faculty of Health and Medical Sciences, University of Copenhagen, Copenhagen, Denmark
[3]Department of Biology, Section for Cell Biology and Physiology, University of Copenhagen, Copenhagen, Denmark
[4]Institute of Sports Medicine Copenhagen, Department of Orthopedic Surgery, Copenhagen University Hospital Bispebjerg and Frederiksberg, Copenhagen, Denmark
[5]Center for Healthy Aging, Department of Clinical Medicine, University of Copenhagen, Copenhagen, Denmark

Corresponding authors: Rasmus Kjøbsted, rasmus.kjobsted@nexs.ku.dk, and Jørgen F.P. Wojtaszewski, jw@nexs.ku.dk

Received 3 August 2022 and accepted 12 April 2023

for the ability of exercise and contraction to enhance whole-body and muscle insulin sensitivity (26). In addition, we have shown that TBC1D4 is necessary for contraction and AICAR (5-aminoimidazole-4-carboxamide-1-β-D-ribofuranoside; AMPK activator) to enhance muscle insulin sensitivity (27), and several human studies have demonstrated enhanced phosphorylation of TBC1D4-S711 concomitant with improved muscle insulin sensitivity after exercise (5,28,29). Together, this inspired us to hypothesize that an AMPK-TBC1D4-S711 signaling axis mediates the beneficial effect of exercise and contraction on muscle insulin sensitivity.

To test our hypothesis, we generated a knock-in mouse model with a point mutation that replaces serine with alanine at residue 711 in the long isoform of *Tbc1d4* (TBC1D4-S711A). Our findings reveal that the lack of phosphorylated TBC1D4-S711 does not affect whole-body and muscle insulin sensitivity in resting mice on either chow or high-fat diets (HFDs). In contrast, TBC1D4-S711A mice do not exhibit enhanced whole-body and muscle insulin sensitivity after exercise and contraction. Collectively, these results suggest that phosphorylation of TBC1D4-S711 is necessary for muscle insulin sensitization after exercise and contraction in mice.

RESEARCH DESIGN AND METHODS

Animal Models

All animal experiments were approved by the Danish Animal Experiments Inspectorate (Copenhagen, Denmark) (permit number 2019-15-0201-01659) and complied with the EU convention for the protection of vertebrates used for scientific purposes. TBC1D4-S711A mice were generated using CRISPR-Cas9 technology as previously described (27). In short, Cas9 protein with a single guide RNA (sgRNA) was used together with a repair template encoding the desired mutations to substitute the S711 codon (TCT) with an alanine codon (GCG) in exon 11 that is present only in the long isoform of *Tbc1d4*. A silent mutation was introduced in the repair template to prevent sgRNA reannealing (Fig. 1*A*). Heterozygous TBC1D4-S711A male and female mice were used to breed wild-type, heterozygous, and homozygous TBC1D4-S711A mice, all of which were

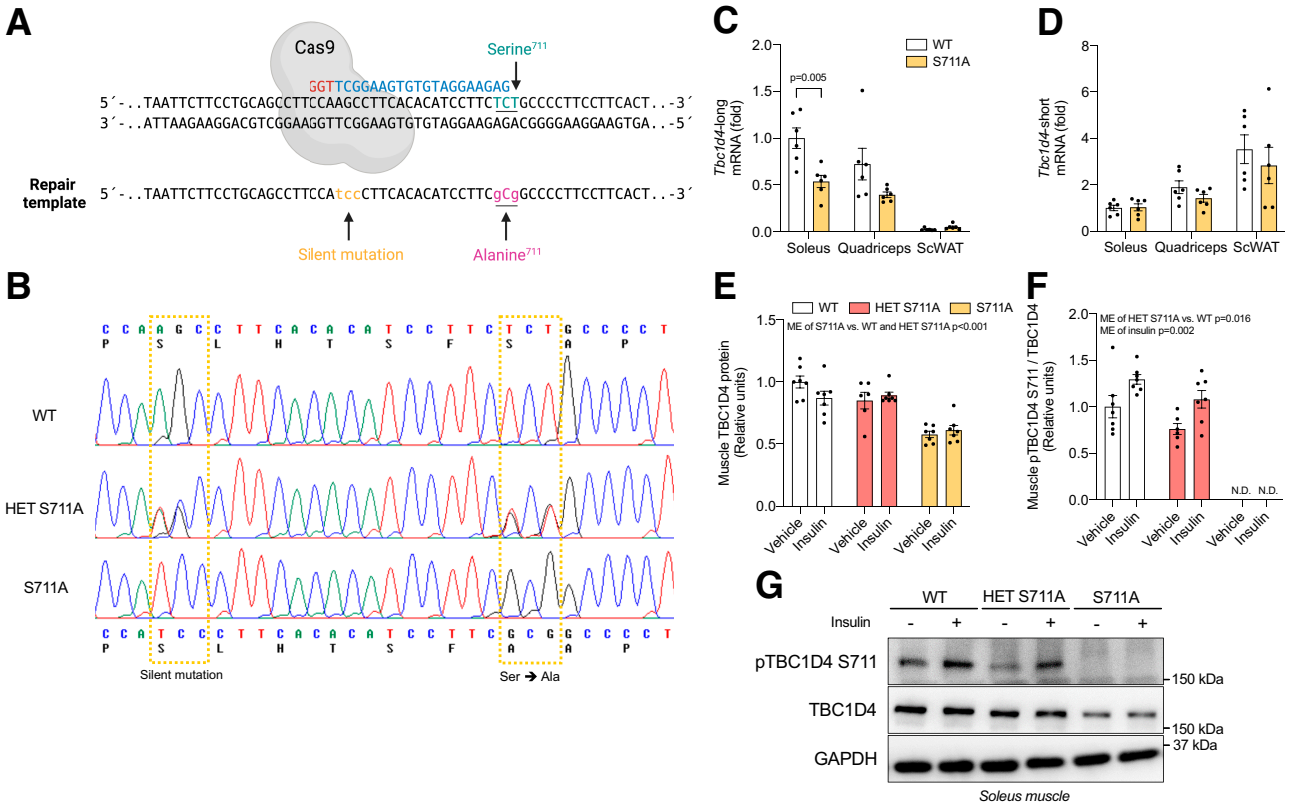

Figure 1—Generation and validation of the TBC1D4-S711A mouse model. *A*: Schematic representation of the CRISPR-Cas9 with designed sgRNA and repair template. Position 711 of the *Tbc1d4* gene is highlighted in green (wild-type) and purple (knock-in), while the silent mutation on position 705 is highlighted in yellow. *B*: Sequencing of the *Tbc1d4* gene around the knock-in and silent mutations in wild-type, heterozygous, and homozygous TBC1D4-S711A mice. *C* and *D*: mRNA content of *Tbc1d4*-long and *Tbc1d4*-short in soleus muscle, quadriceps muscle, and subcutaneous white adipose tissue (ScWAT) from wild-type and TBC1D4-S711A mice. *E* and *F*: Quantification of TBC1D4 protein and phosphorylated (p) TBC1D4-S711 in soleus muscle dissected from anesthetized mice 15 min after a retro-orbital injection of vehicle (0.9% saline) with or without insulin (0.75 units/kg). *G*: Representative immunoblots. Data were analyzed by a Student *t* test (*C* and *D*) and a two-way ANOVA (*E* and *F*). Dots represent individual values, while bar graphs represent means ± SEM (n = 6–7). ME, main effect; N.D., not detected; WT, wild type.

fertile and viable. To ensure correct mutagenesis, the three different genotypes were sequenced around the mutated codons (Fig. 1*B*) and subsequently genotyped using the following PCR primer sets: WT: FP 5′-GAGTAATTCTTCCTGCAGCCTTCCAA-3′ and RP 5′-GGAGCAGTGAAGGAAGGGGCAGAG-3′; and S711A: FP 5′-GAGTAATTCTTCCTGCAGCCTTCCATC-3′ and RP 5′-GCAGTGAAGGAAGGGGCCG-3′. Heterozygous long isoform–specific TBC1D4 knockout (KO) mice were also generated, genotyped, and used as previously described (27). Mice were bred at the Department of Experimental Medicine, University of Copenhagen, and housed with nesting material in temperature- and humidity-controlled rooms on a 12:12-h light-dark cycle (lights on 06:00 A.M.) with free access to standard rodent chow diet (Altromin #1324) and water. All experiments were performed on female mice unless stated otherwise.

Body Weight, Body Composition, and Food Intake

Body weight and food intake were recorded once weekly using a precision scale. Lean mass and fat mass were measured at the end of the diet interventions using an EchoMRI 4in1 Body Composition Analyzer.

HFD Intervention

Eleven- to thirteen-week-old mice were single-caged and provided free access to an HFD (60% calories from fat; Research Diets #D12492) for 14 weeks.

Glucometabolic Studies

For fasting and refeeding experiments, fed blood glucose concentrations were measured in single-housed mice at ∼07:00 A.M. Fasting and refeeding blood glucose concentrations were measured in mice fasted 16 h overnight (start ∼03:00 P.M.) as well as 30 and 60 min after being given free access to standard chow diet. For the oral glucose tolerance test (OGTT), single-housed mice were fasted 16 h overnight (start ∼03:00 P.M.) after which D-glucose (2 g/kg body weight) dissolved in saline (0.9%) was administered by oral gavage. For the insulin tolerance test (ITT), single-housed mice were fasted 4 h (start ∼07:00 A.M.), after which insulin (0.75 units/kg, Actrapid; Novo Nordisk) dissolved in saline (0.9%) was administered by a single intraperitoneal injection. Blood glucose levels were determined at t = 0, 15, 30, 45, 60, and 120 min during the OGTT and ITT. At all time points during the fasting refeeding experiments as well as at t = 0, 15, and 30 min during the OGTT, ∼35 μL blood was drawn into heparinized capillary tubes to determine insulin concentrations in plasma, which was prepared from whole blood centrifugation (16,000 *g* for 5 min at 4°C). HOMA-IR (homeostatic model assessment for insulin resistance) was calculated from the following equation: HOMA-IR = Fasting plasma insulin · Fasting blood glucose/22.5.

Plasma Insulin, Blood Glucose, and Blood Lactate

Handheld glucose (Contour XT; Bayer) and lactate (Lactate Plus; Nova Biomedical) analyzers were used for all blood glucose and lactate measurements that were sampled from the tail vein. Plasma insulin was determined using an ELISA kit from ALPCO (80-INSMSU-E10).

Muscle Glycogen

Muscle glycogen was measured on whole muscle homogenate after acid hydrolysis and determined by a fluorometric method (30).

Real-Time PCR

Procedures for isolation of RNA and reverse transcription have been described previously (31). The mRNA content of the short and long isoform of TBC1D4 was determined by real-time PCR using SYBR Green (SYBR Green PCR Master Mix; Thermo Fischer Scientific, Woolston Warington, U.K.). PCR primer set for the short and long isoform of the mouse *Tbc1d4* gene (short: FP 5′-TCCAGCGAACAATGCAGTGA-3′ and RP 5′-GATGCAACCCGGAGGAAAAT-3′; long: FP 5′-CAGCCCGGCGCATGTA-3′ and RP 5′-CAGGAAAGAGGGAGCAGTGAA-3′) was designed using Primer Express software (Applied Biosystems, Thermo Fisher Scientific, Waltham, MA) and obtained from TagCopenhagen (Copenhagen, Denmark). A serial dilution was made separately for subcutaneous white adipose tissue (ScWAT) and skeletal muscle cDNA samples and used to construct tissue-specific standard curves. These were used to convert the cycle threshold values of the unknown samples, taking into account tissue-specific PCR efficiency, while the *y*-axis intersect value of the muscle standard curve was used for both muscle and ScWAT to obtain comparable mRNA levels. The amount of TBC1D4 mRNA was normalized to the average amount of β-actin and TBP mRNA of each cDNA sample. The β-actin and TBP mRNA were determined using predeveloped assay reagents and Universal Mastermix (Applied Biosystems) and were not affected by the genotype (32). The amount of TBC1D4 mRNA is, in all three tissues, presented as fold-change relative to the level in soleus muscle from wild-type mice, which was set to one.

In Vivo Insulin-Stimulated Tissue Glucose Clearance

Fed and single-housed mice were anesthetized by a single intraperitoneal injection of pentobarbital and xylocain (90 mg/kg and 5 mg/kg, respectively) and left to recover for 15 min. Subsequently, a bolus of saline (0.9%) with or without insulin (0.75 units/kg), containing [^{3}H]-2-deoxyglucose (66.7 uCi/mL) (Hartmann Analytic, Braunschweig, Germany), was administered by a single retro-orbital intravenous injection. Blood glucose concentrations were determined at t = 0, 5, 10, and 15 min. Moreover, 25 μL blood was collected at similar time points to determine the specific activity of [^{3}H]-2-deoxyglucose in plasma. Tissues were collected at t = 15 min after euthanization of animals by cervical dislocation to determine phosphorylated [^{3}H]-2-deoxyglucose ([^{3}H]-2-deoxy-glucose-6-P) tissue content as previously described (33). Tissue glucose clearance rates (mL blood · g tissue^{-1} · min^{-1}) were calculated by relating the amount of [^{3}H]-2-deoxy-glucose-6-P

accumulated in tissues to the tissue weight, the specific activity in plasma, the time of exposure, and the average blood glucose concentration.

Ex Vivo Insulin- and AICAR-Stimulated Muscle Glucose Uptake

Insulin- and AICAR-stimulated glucose uptake was determined in isolated skeletal muscle using a previously described technique (34). Although AICAR is an unspecific AMPK activator that promotes intracellular accumulation of ZMP (AICAR monophosphate), the effect of AICAR on muscle glucose uptake has repeatedly been shown to be dependent on AMPK (35–37). Fed animals were anesthetized by a single intraperitoneal injection of pentobarbital and xylocain (100 and 5 mg/kg, respectively) after which soleus and extensor digitorum longus (EDL) were removed and suspended in heated (30°C) and continuously gassed (95% O_2 and 5% CO_2) incubation chambers (Multi Myograph System; Danish Myo Technology, Aarhus, Denmark) containing Krebs Ringer buffer supplemented with 0.1% BSA, 8 mmol/L mannitol, and 2 mmol/L pyruvate (KRB). After 10 min preincubation in KRB, muscles were incubated for 30 min in KRB containing AICAR (2 mmol/L) (Toronto Research Chemicals, Toronto, Ontario, Canada) or insulin (100 or 10,000 μU/mL) (Actrapid; Novo Nordisk, Denmark). The uptake of 2-deoxyglucose was measured during the last 10 min of the 30-min stimulation period by adding 1 mmol/L [^{3}H]-2-deoxyglucose (0.056 MBq/mL), 7 mmol/L [^{14}C]-mannitol (0.0167 MBq/mL) (Hartmann Analytic, Braunschweig, Germany), and 2 mmol/L pyruvate to the incubation medium. After incubation, muscles were washed in ice-cold KRB, dried on filter paper, and frozen in liquid nitrogen. Glucose uptake was assessed by the accumulation of [^{3}H]-2-deoxyglucose in muscle by using [^{14}C]-mannitol as an extracellular marker. Radioactivity was measured in muscle lysates using liquid scintillation counting (Ultima Gold and Tri-Carb 4910 TR; PerkinElmer) and related to the specific activity of the incubation buffer.

In Situ Contraction-Stimulated Muscle Glucose Uptake

In situ contraction-stimulated muscle glucose uptake was determined as previously described (26,38). In short, an electrode was placed on the common peroneal nerve of one leg of fed mice that had been anesthetized by a single intraperitoneal injection of pentobarbital and xylocain (100 and 5 mg/kg, respectively). The contralateral leg served as a sham-operated resting control. Muscle glucose uptake during 10 min of electrical stimulation was determined by retroorbital injection of [^{3}H]-2-deoxyglucose as described above, with blood sampling and blood glucose determination at t = 0, 5, and 10 min. For measurements of muscle glucose uptake after contraction, anesthetized and muscle-contracted mice were left to recover on a heating plate (30°C) for 30 min, after which muscle glucose uptake was determined during a 10-min stimulation period as described above.

Insulin-Stimulated Muscle Glucose Uptake After In Situ Contraction

Measurements of insulin sensitivity in isolated EDL muscle after in situ contraction were performed as previously described (26), except that EDL muscles were allowed to recover in incubation chambers for 2 h. In short, EDL muscles were excised immediately after in situ contraction and suspended in heated (30°C) and continuously gassed (95% O_2 and 5% CO_2) incubation chambers containing KRB supplemented with 5 mmol/L D-glucose and 5 mmol/L mannitol. Following a 2-h recovery period, basal and submaximal (100 μU/mL) insulin-stimulated 2-deoxyglucose uptake were assessed in EDL muscles during the last 10 min of a 30-min stimulation period as described above. These experiments were performed separately in both male and female mice.

ITT After Exercise

Measurements of insulin tolerance after a single bout of exercise were performed as previously described (26). In short, following treadmill running acclimatization on five consecutive days, mice were subjected to a graded maximal running test to assess the maximal running speed of each individual mouse. Blood glucose and lactate concentrations were measured immediately before and after the maximal running test in a subgroup of animals. For ITTs, mice were single-housed and fasted for 2 h (start ∼06:00 A.M.) before performing 30 min of treadmill exercise (55% of individual maximal running speed). Resting control mice were left in their cages. Immediately after exercise, mice returned to their individual cages for 1 h without access to food and were subsequently administered with a submaximal dose of insulin (0.3 units/kg) dissolved in saline (0.9%) by a single intraperitoneal injection. Blood glucose concentrations were determined at t = 0, 20, 40, 60, 90, and 120 min.

Muscle Processing and Western Blot Analyses

Tissues were crushed in liquid nitrogen prior to homogenization, except for soleus and EDL muscle. Tissues were homogenized in ice-cold lysis buffer as previously described (39) and subsequently rotated end over end for 1 h at 4°C to increase protein extraction. Portions of the homogenate were centrifuged at 16,000 g for 20 min at 4°C, after which the supernatant (lysate) was collected. Total protein abundance in tissue lysates and homogenates was determined in triplicates by the bicinchoninic acid method (Thermo Fisher Scientific, Waltham, MA). Equal amounts of muscle protein lysate were heated in Laemmli buffer (96°C, 10 min) before being subjected to SDS-PAGE and Western blotting analyses as previously described (39).

AMPK Activity

AMPKα2β2γ3-, α2βγ1-, and α1βγ1-associated activity was determined in muscle protein lysate by three consecutive immunoprecipitations using custom-made anti-AMPKγ3, anti-AMPKα2, and anti-AMPKα1 as previously described (40).

Antibodies

Anti-TBC1D4-pT649 (no. 8881), anti-Akt2 (no. 3063), anti-Akt-pS473 (no. 9271), anti-Akt-pT308 (no. 9275), anti-ACC-pS212 (no. 3661), anti-AMPKα-pT172 (no. 2531), anti-p38-MAPK (no. 9212), and anti-GAPDH (no. 2118) were all from CST (Danvers, MA). Anti-TBC1D1-pS231 (no. 07-2268) was from Millipore (Burlington, MA), anti-GLUT4 (PA1-1065) was from Thermo Fischer Scientific (Waltham, MA), and anti-AMPKα2 (sc-19131) and anti-hexokinase-II (sc-130358) were from Santa Cruz Biotechnology (Dallas, TX). Anti-TBC1D4 (ab189890) and anti-TBC1D1 (ab229504) were from Abcam (Cambridge, U.K.), and ACC protein was detected using horseradish peroxidase–conjugated streptavidin (P0397) from Agilent (Santa Clara, CA). Anti-TBC1D4-pS711 was custom made by Capra Science (41).

Statistical Analyses

The statistical analyses were performed using GraphPad Prism software (GraphPad Software, San Diego, CA). Data are presented with individual values, while bar and line graphs represent means ± SEM unless stated otherwise. An unpaired two-tailed Student *t* test was used for two-group comparisons. Two independent variables were compared using two-way ANOVAs with or without repeated measures, followed by Sidak's multiple comparisons test when an interaction between variables occurred. When unequal variance was observed between groups, the data were $\log_{10}$ transformed to obtain equal variance. Statistical significance was defined as $P < 0.05$.

Data and Resource Availability

The data and resources generated and/or analyzed during the current study are available from the corresponding authors on reasonable request.

RESULTS

The TBC1D4-S711A Mutation Decreases TBC1D4 mRNA and Protein Levels in Skeletal Muscle

Initial investigations revealed that the TBC1D4-S711A mutation decreased mRNA levels of the long isoform of *Tbc1d4* by ∼40–50% in muscle whereas the short isoform of *Tbc1d4* remained unaffected in both muscle and ScWAT from homozygous TBC1D4-S711A mice (Fig. 1*C* and *D*). This led to a decrease in TBC1D4 protein content in skeletal muscle from homozygous TBC1D4-S711A mice (Fig. 1*E*), because skeletal muscle predominantly expresses the long isoform of *Tbc1d4* (42). In addition, we found that basal and insulin-stimulated phosphorylation of TBC1D4-S711 was reduced in muscle from heterozygous TBC1D4-S711A mice and absent in muscle from homozygous TBC1D4-S711A mice (Fig. 1*F* and *G*). These data validate the TBC1D4-S711A mouse model and provide an opportunity to investigate the importance of TBC1D4-S711 for the regulation of muscle insulin sensitivity and whole-body glycemic control.

Whole-Body Glycemic Control Is Not Affected in TBC1D4-S711A Mice

Analyses of chow-fed homozygous female TBC1D4-S711A mice revealed no phenotype regarding body weight, body composition, and food intake when compared with wild-type littermates (Fig. 2*A–C*). TBC1D4-S711A mice displayed normal blood glucose and plasma insulin levels in the fed and fasted states (Fig. 2*D* and *E*). HOMA-IR levels (Fig. 2*F*) implied that the TBC1D4-S711A mice exhibited intact whole-body insulin sensitivity. This was supported by a comparable increase in postprandial blood glucose and plasma insulin levels in the two genotypes 30 and 60 min after refeeding (Fig. 2*D* and *E*), as well as similar glucose and insulin tolerance (Fig. 2*G–I*). Together, these data demonstrate that the TBC1D4-S711A mutation does not affect whole-body glycemic control in resting lean female mice.

In Vivo Insulin-Stimulated Muscle Glucose Clearance Is Not Impaired in TBC1D4-S711A Mice

Mice with a TBC1D4-T649A mutation have reduced rates of insulin-stimulated muscle glucose uptake (19). Therefore, we decided also to investigate the effect of the TBC1D4-S711A mutation on in vivo insulin-stimulated glucose clearance. Retro-orbital intravenous injection of insulin decreased blood glucose levels and increased glucose clearance in skeletal muscle and ScWAT to a similar extent in TBC1D4-S711A and wild-type mice (Fig. 3*A–D*). These findings were associated with intact proximal insulin signaling in ScWAT and muscle (Akt-T308/S473) but lower phosphorylation of TBC1D4-T649 in muscle from TBC1D4-S711A mice due to decreased TBC1D4 protein levels (Fig. 3*E–N*). This demonstrates that phosphorylation of TBC1D4-S711 is dispensable for in vivo insulin-stimulated muscle glucose clearance during resting conditions.

Insulin- and AICAR-Stimulated Glucose Uptake Is Not Compromised in Isolated Oxidative and Glycolytic Skeletal Muscle From TBC1D4-S711A Mice

To circumvent potential humoral factors that may affect muscle glucose uptake in the in vivo mouse model, we examined the ability of insulin and AICAR to increase glucose uptake in isolated soleus (oxidative) and EDL (glycolytic) muscle. Upon submaximal and maximal insulin stimulation, glucose uptake rates increased to a similar extent in soleus and EDL muscle from TBC1D4-S711A and wild-type mice (Fig. 4*A* and *B*). The effect of AICAR on glucose uptake did not differ between genotypes (Fig. 4*A* and *B*). We confirmed that insulin increased phosphorylation of Akt-T308/S473 and AICAR increased phosphorylation of TBC1D1-S231 and ACC-S212 similarly in muscle from the two genotypes (Fig. 4*C–J*). Insulin-stimulated phosphorylation of TBC1D4-T649 was reduced in muscle from TBC1D4-S711A mice due to decreased TBC1D4 protein levels (Fig. 4*K–O* and *Q*). Insulin and AICAR increased phosphorylation of TBC1D4-S711 in muscles from wild-type mice (Fig. 4*P*, *R*, and *S*).

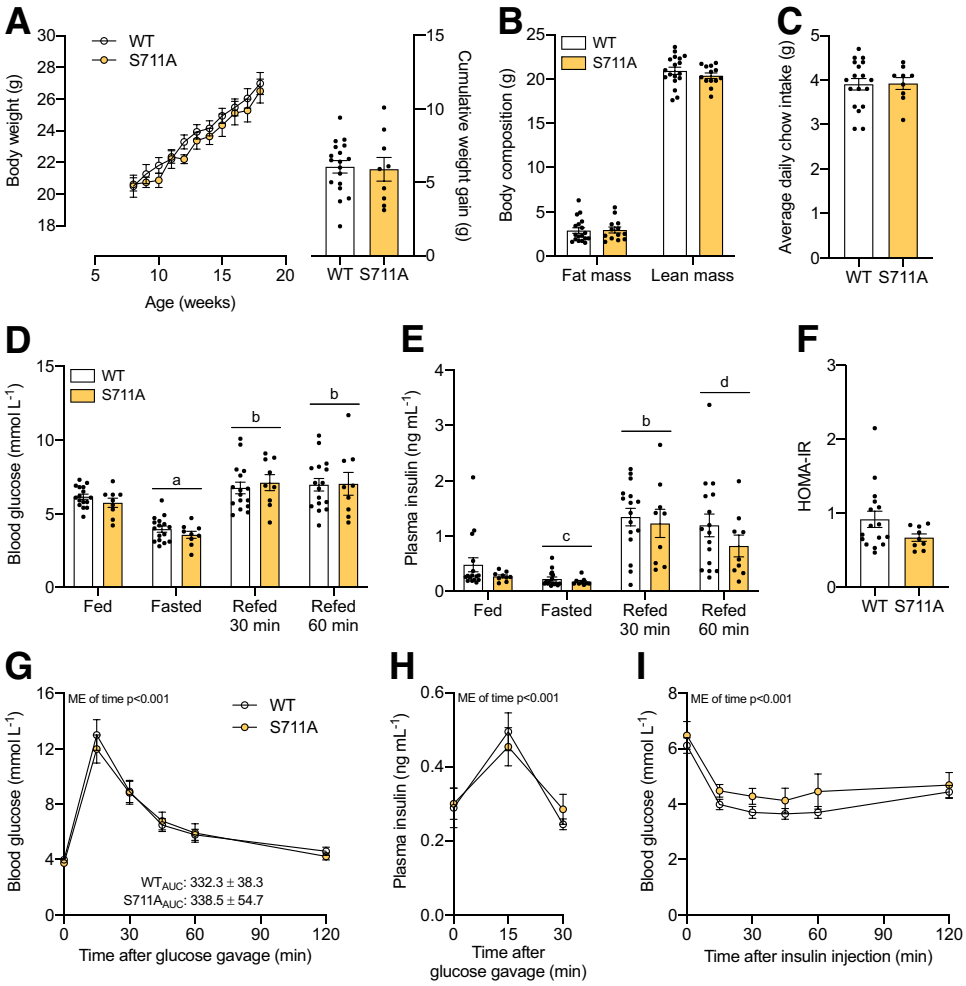

Figure 2— Whole-body glycemic control is not affected in resting TBC1D4-S711A female mice on chow diet. *A*: Body weight (left) and cumulative weight gain (right) in wild-type and TBC1D4-S711A chow-fed mice between 8 and 18 weeks of age. *B*: Body composition in 16- to 17-week-old mice. *C*: Average daily chow intake in mice between 8 and 18 weeks of age. *D* and *E*: Blood glucose and plasma insulin concentrations measured in the morning after having free access to chow diet (fed), following an overnight fast (16 h) (fasted), as well as 30 and 60 min after refeeding with regular chow diet following the overnight fast in 9- to 10-week-old wild-type and TBC1D4-S711A mice; a indicates $P <$ 0.001 versus all groups, b indicates $P < 0.05$ versus fed group, c indicates $P < 0.001$ versus refed groups, and d indicates $P < 0.01$ versus fed group. *F*: HOMA-IR levels determined from the fasting blood glucose and plasma insulin concentrations in *D* and *E*. *G* and *H*: Blood glucose and plasma insulin concentrations during an OGTT (2 g/kg) in 11- to 12-week-old wild-type and TBC1D4-S711A mice. Glucose area under the curve (AUC) values during the OGTT are shown in *G*. *I*: Blood glucose concentrations during an ITT (0.75 units/kg) in 15- to 16-week-old wild-type and TBC1D4-S711A mice. Data were analyzed by a Student *t* test (*A–C*) and a two-way repeated ANOVA (*D–I*). Dots represent individual values, while bar and line graphs represent means ± SEM (n = 15–18 in wild-type and n = 8–13 in TBC1D4-S711A groups). Data in *G* were transformed to obtain equal variance prior to statistical testing. ME, main effect; WT, wild type.

Whole-Body Glycemic Control Is Not Impaired in TBC1D4-S711A Mice on HFD

To evaluate the potential detrimental effect of the TBC1D4-S711A mutation on whole-body glycemic control in an obesogenic environment, female TBC1D4-S711A mice and wild-type littermates were exposed to a standard HFD for 14 weeks. To our surprise, TBC1D4-S711A mice gained slightly less weight and displayed reduced body fat content when fed an HFD (Fig. 5*A* and *B*), although food intake was comparable in the two genotypes (Fig. 5*C*). Despite this, no differences in blood glucose and plasma insulin levels were observed between genotypes in the fed, overnight fasted, and refed states (Fig. 5*D* and *E*), nor did HOMA-IR and glucose tolerance differ (Fig. 5*F–H*). In agreement, insulin decreased blood glucose levels and stimulated glucose uptake in skeletal muscle and ScWAT to a similar extent in the two genotypes on an HFD (Fig. 5*I–L*). These findings were associated with comparable insulin-related tissue signaling (Fig. 5*M–V*). Collectively, our observations demonstrate that the TBC1D4-S711A mutation is not important for regulating whole-body and muscle glucose metabolism in resting obese female mice.

Contraction-Induced Glucose Uptake and AMPK Activity Are Not Impaired in Muscle From TBC1D4-S711A Mice

Recent evidence supports a role of AMPK in regulating muscle glucose uptake in the immediate period after exercise

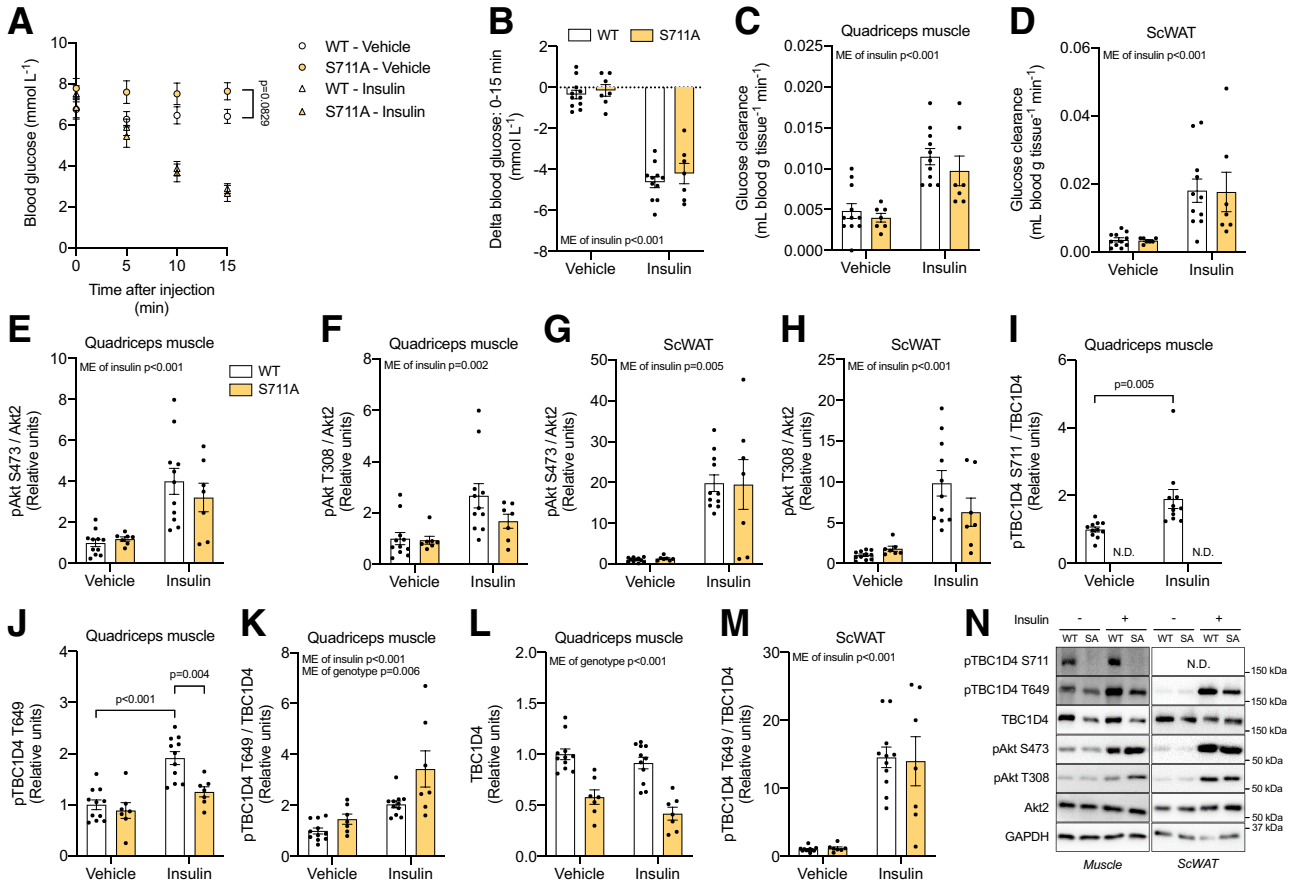

Figure 3—In vivo insulin-stimulated glucose uptake is not impaired in muscle and adipose tissue from TBC1D4-S711A female mice. *A* and *B*: Blood glucose and changes in blood glucose concentrations in anesthetized 17- to 18-week-old wild-type and TBC1D4-S711A mice following retro-orbital injection of vehicle (0.9% saline) with or without insulin (0.75 units/kg). *C* and *D*: In vivo insulin-stimulated glucose uptake in quadriceps muscle and subcutaneous white adipose tissue (ScWAT) from wild-type and TBC1D4-S711A mice. *E–M*: Insulin-stimulated signaling in quadriceps muscle and ScWAT from wild-type and TBC1D4-S711A mice measured at the level of phosphorylated (p) Akt and TBC1D4. *N*: Representative immunoblots. Data were analyzed by a two-way repeated ANOVA within treatments (*A*), a two-way ANOVA between genotypes (*B–H* and *J–M*) and a Student *t* test (*I*). Dots represent individual values, while bar and line graphs represent means ± SEM ($n = 11$ in wild-type and $n = 7$ in TBC1D4-S711A groups). Data in *D–F* and *M* were transformed to obtain equal variance prior to statistical testing. ME, main effect; N.D., not detected; WT, wild type; SA, S711A.

and contraction (38). Therefore, we investigated the importance of the AMPK-TBC1D4-S711 signaling axis for the regulation of muscle glucose uptake in response to contraction. Glucose uptake was not impaired during contraction or 30 min after contraction in skeletal muscle from TBC1D4-S711A mice (Fig. 6*A* and *B*). In response to contraction, glycogen levels decreased (Fig. 6*C*) whereas AMPK activity and downstream signaling increased to a similar extent in muscle from the two genotypes (Fig. 6*D–G*). Phosphorylation of TBC1D4-S711 increased by contraction in wild-type muscle (Fig. 6*H* and *I*). These findings suggest that AMPK-mediated phosphorylation of TBC1D4-S711 is not involved in regulating muscle glucose uptake in response to contraction and that the applied contraction protocol elicits a comparable metabolic stress in muscle from the two genotypes.

The TBC1D4-S711A Mutation Disrupts Improvements in Muscle Insulin Sensitivity After Contraction

Because both insulin and exercise-induced AMPK activation converge on TBC1D4-S711 to promote its phosphorylation (21) and insulin-stimulated phosphorylation of TBC1D4-S711 is elevated in prior exercised and insulin-sensitized skeletal muscle (5,28,29), we tested the importance of TBC1D4-S711 for improving muscle insulin sensitivity after contraction. Two hours after contraction, insulin-independent glucose uptake was not significantly different between prior contracted and rested muscles (Fig. 7*A* and *B*). However, prior contraction increased submaximal insulin-stimulated glucose uptake in isolated muscle from wild-type mice (Fig. 7*A*) but failed to do so in muscle from TBC1D4-S711A mice (Fig. 7*B*). Accordingly, the incremental increase (delta) in insulin-stimulated glucose uptake (glucose uptake of non-insulin-stimulated muscles subtracted from glucose uptake of paired insulin-stimulated muscles) was only elevated after prior contraction in muscle from wild-type mice (Fig. 7*C*).

Because our findings were derived from experiments in female mice, we wanted to test whether male TBC1D4-S711A mice exhibited a similar phenotype. We observed that the ability of contraction to improve insulin-stimulated glucose uptake was disrupted in muscle from male TBC1D4-S711A

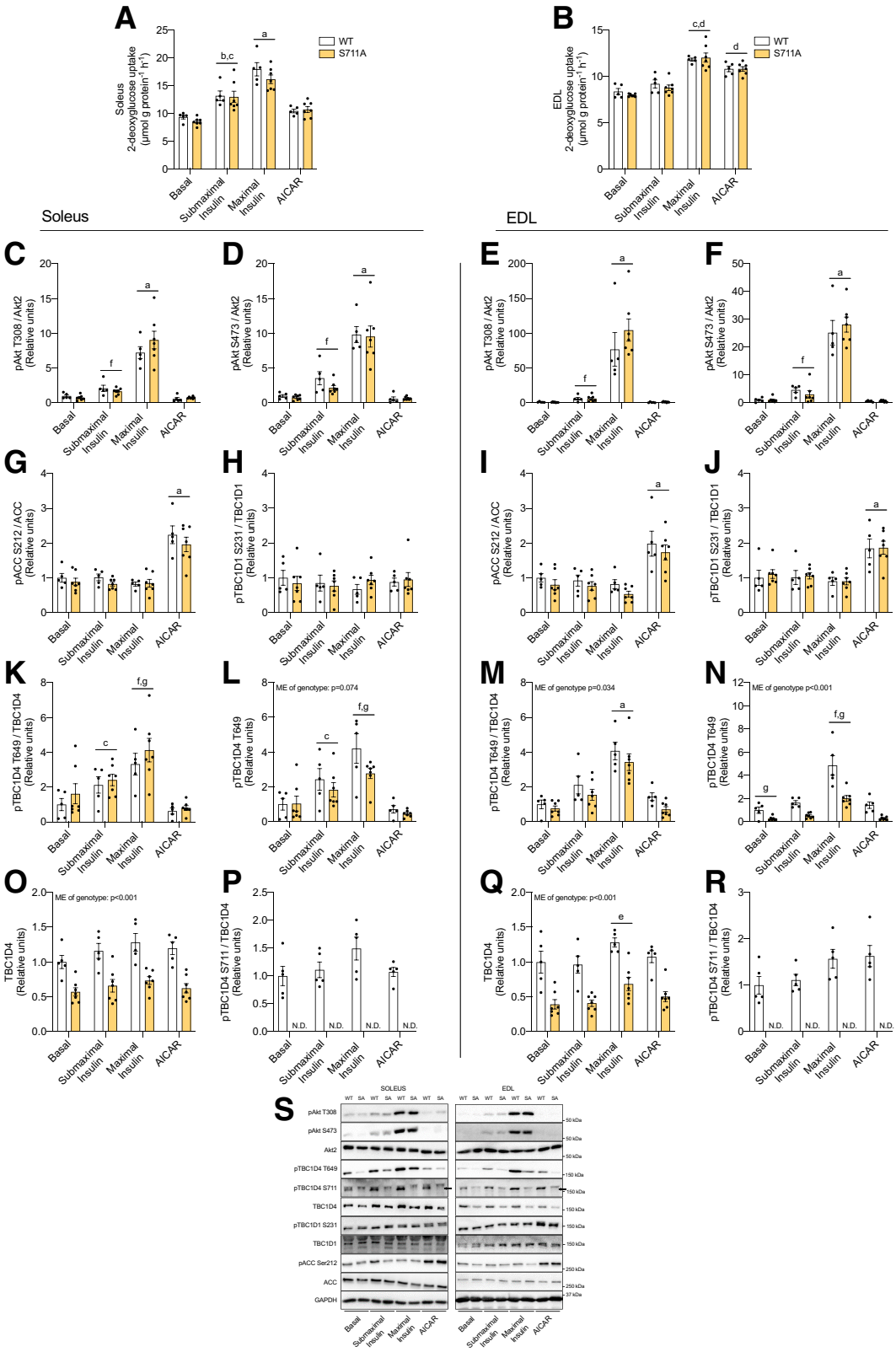

Figure 4—Insulin- and AICAR-stimulated glucose uptake is not impaired in isolated skeletal muscle from TBC1D4-S711A female mice. *A* and *B*: Basal, submaximal insulin- (100 μU/mL), maximal insulin- (10,000 μU/mL), and AICAR-stimulated glucose uptake in isolated soleus and EDL muscle from wild-type and TBC1D4-S711A mice. *C–R*: Protein content of TBC1D4 as well as insulin- and AICAR-stimulated phosphorylation (p) of Akt-T308, Akt-S473, TBC1D1-S231, ACC-212, TBC1D4-T649, and TBC1D4-S711 measured in muscles from *A* and *B*; a indicates $P < 0.001$ versus all groups, b indicates $P < 0.001$ versus basal, c indicates $P < 0.05$ versus AICAR, d indicates $P < 0.001$ versus basal and submaximal insulin, e indicates $P < 0.05$ versus basal and submaximal insulin, f indicates $P < 0.001$ versus basal

mice (Fig. 7*D* and *E*). However, there was a tendency for improved muscle insulin sensitivity in male TBC1D4-S711A mice ($P = 0.061$) (Fig. 7*F*), suggesting that male TBC1D4-S711A mice retain the ability to increase muscle insulin sensitivity after contraction but less markedly than male wild-type mice.

To investigate whether the reduced abundance of TBC1D4 protein was affecting the observations in muscle from female TBC1D4-S711A mice, we tested the ability of contraction to improve muscle insulin sensitivity in heterozygous muscle-specific TBC1D4 KO female mice in which muscle TBC1D4 protein is reduced by ~50%. Importantly, prior contraction improved muscle insulin sensitivity in these mice (Fig. 7*G* and *H*), suggesting that the inability of contraction to improve muscle insulin sensitivity in female TBC1D4-S711A mice is not due to a reduced abundance of muscle TBC1D4 protein.

GLUT4 and Hexokinase-II protein levels, as well as proximal insulin signaling measured at the level of Akt-T308, were similar in EDL muscles from wild-type and TBC1D4-S711A female mice (Fig. 7*I–K*). Insulin increased phosphorylation of TBC1D4-T649 in muscle from both genotypes (Fig. 7*L*), while phosphorylation of TBC1D4-T649 related to TBC1D4 protein was slightly increased by prior contraction in wild-type muscle only (Fig. 7*M* and *N*). Importantly, insulin-stimulated phosphorylation of TBC1D4-S711 was elevated in prior contracted and insulin-sensitized EDL muscle from wild-type mice (Fig. 7*O* and *P*), which further supports a role of TBC1D4-S711 in regulating muscle insulin sensitivity.

The TBC1D4-S711A Mutation Disrupts Improvements in Whole-body Insulin Sensitivity After a Single Bout of Exercise

To address the physiological relevance of TBC1D4-S711 for the regulation of muscle insulin sensitivity, we examined in vivo whole-body insulin sensitivity in mice by an intraperitoneal injection of a submaximal insulin dose (0.3 units/kg) after a single bout of treadmill exercise. Initial findings revealed that the maximal running capacity did not differ between genotypes (Fig. 8*A*) nor did the blood glucose and lactate levels before and after the maximal running test (Fig. 8*B* and *C*). Prior exercise enhanced the blood glucose–lowering effect of insulin only in wild-type mice, and thus, improved whole-body insulin tolerance by ~75% in wild-type mice (Fig. 8*D–F*). This provides further evidence to support that TBC1D4-S711 is a key phosphorylation site essential for enhancing muscle insulin sensitivity after exercise to improve whole-body glycemic control.

DISCUSSION

Previously, we have shown that AMPK and TBC1D4 are necessary for improving muscle insulin sensitivity after contractions and that phosphorylation of TBC1D4-S711 is enhanced in prior contracted and insulin-sensitized muscle (26,27). Using mice harboring a single TBC1D4-S711A point mutation, we now show that phosphorylation of TBC1D4-S711 is necessary for improving muscle insulin sensitivity after contractions and whole-body insulin sensitivity after a single bout of exercise.

We found that the mRNA level and protein abundance of TBC1D4 were decreased by ~50% in skeletal muscle from TBC1D4-S711A mice. We believe that the observed decrease in muscle TBC1D4 protein is a consequence of a decrease in the TBC1D4 mRNA levels. This may be explained by the introduced gene mutations that can interfere with the ability of exonic splicing enhancers to promote efficient gene splicing (43). Gene mutations and alterations in a nucleic acid sequence have also been shown to change the secondary structure of mRNA that may create unstable mRNA and lead to premature mRNA degradation of *Tbc1d4* (44). Alternatively, phosphorylation of TBC1D4-S711 may, in itself, regulate the transcription of *Tbc1d4*. Importantly, the decrease in muscle TBC1D4 protein did not affect muscle and whole-body glucose metabolism in chow- or HFD-fed TBC1D4-S711A mice compared with wild-type littermates. To our knowledge, observations from heterozygous TBC1D4 KO mice have not been reported, but heterozygous carriers of a common Greenlandic Inuit loss-of-function mutation in *Tbc1d4* that decreases TBC1D4 protein abundance in muscle by ~50% are not characterized by impaired glucose tolerance or increased risk of type 2 diabetes in contrast to homozygous carriers (45). Together, this suggests that the ~50% reduction in TBC1D4 protein does not compromise muscle and whole-body glucose metabolism during insulin stimulation.

We have recently shown that AMPK and its downstream target TBC1D1 are involved in maintaining muscle glucose uptake elevated in the period after contraction and exercise (38). Because parts of TBC1D1 and TBC1D4 are in complex in skeletal muscle (46), we hypothesized that phosphorylation of TBC1D4-S711 by AMPK could also be involved in regulating muscle glucose uptake after contraction. Nevertheless, our findings did not support TBC1D4-S711 having such a role; therefore, we now propose that AMPK promotes insulin-independent muscle glucose uptake in the immediate period after exercise/contraction via TBC1D1 and it enhances muscle insulin sensitivity several hours after exercise/contraction via TBC1D4.

Improvements in muscle insulin sensitivity after a single bout of exercise in humans are associated with enhanced insulin-stimulated phosphorylation of TBC1D4 (5,28,29). Furthermore, improvements in muscle insulin sensitivity after

and AICAR, and g indicates $P < 0.05$ versus submaximal insulin. *S*: Representative immunoblots. Data were analyzed by a two-way ANOVA, except for data in *P* and *R* that were analyzed by a one-way ANOVA. Dots represent individual values, while bar graphs represent means ± SEM ($n = 5$ in wild-type and $n = 7$ in TBC1D4-S711A groups). An unspecific band is observed in the TBC1D4-S711 immunoblot. Only the specific TBC1D4-S711 band (lower) has been quantified. Data in *C–F* and *N* were transformed to obtain equal variance prior to statistical testing. ME, main effect; N.D., not detected; WT, wild type; SA, S711A.

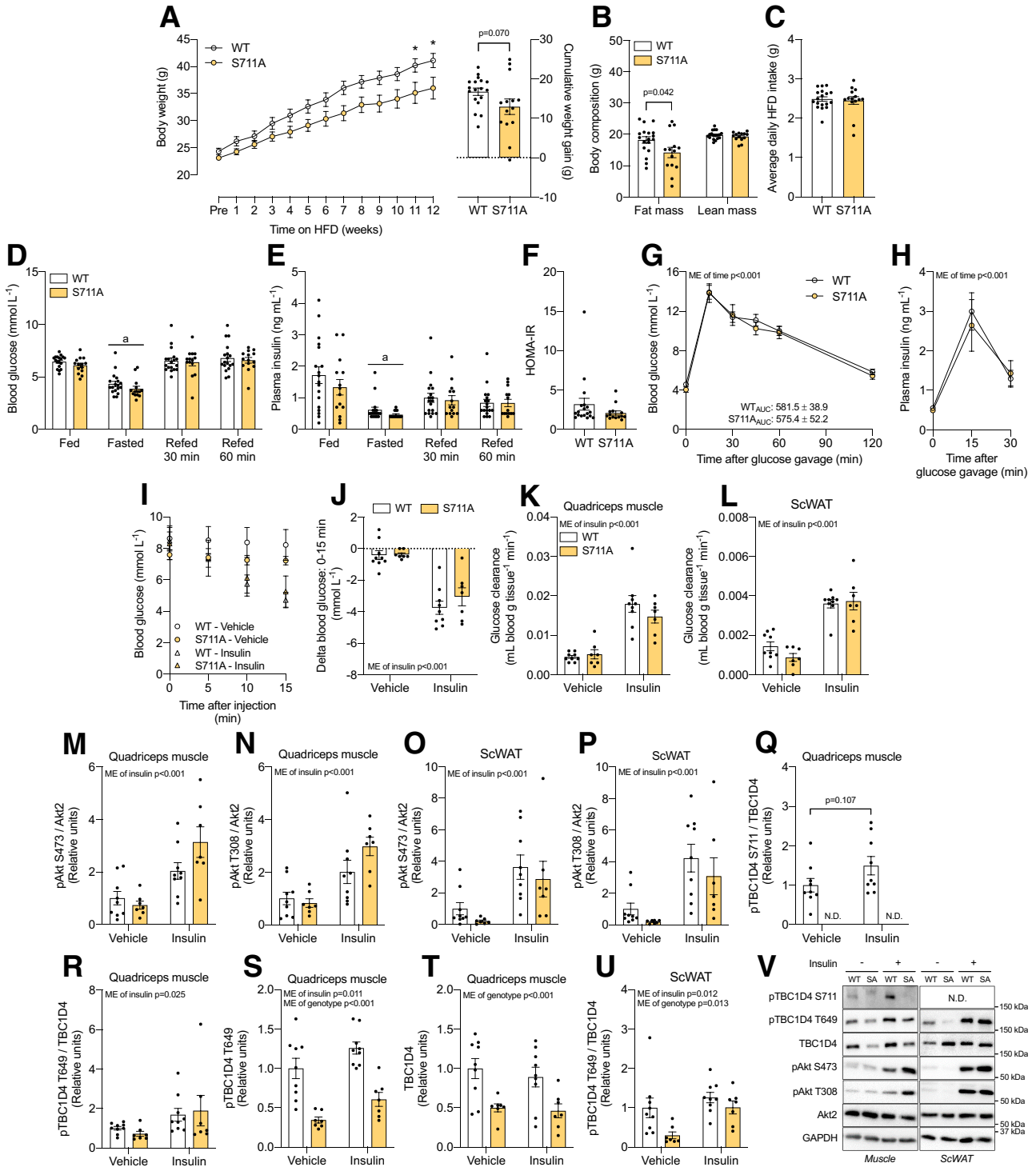

Figure 5—Whole-body glycemic control is not affected in resting HFD-fed TBC1D4-S711A female mice. *A*: Body weight (left) and cumulative weight gain (right) in wild-type and TBC1D4-S711A mice during HFD feeding. Mice were 11–13 weeks old at the beginning of the HFD intervention. *B*: Body composition in HFD-fed mice. *C*: Average daily HFD intake during the diet intervention. *D* and *E*: Blood glucose and plasma insulin concentrations measured in 23- to 25-week-old HFD-fed wild-type and TBC1D4-S711A mice in the morning after having free access to HFD (fed), following an overnight fast (16 h) (fasted) as well as 30 and 60 min after refeeding with regular chow diet following the overnight fast; a indicates $P < 0.001$ versus all groups. *F*: HOMA-IR levels determined from the fasting blood glucose and plasma insulin concentrations in *D* and *E*. *G* and *H*: Blood glucose and plasma insulin concentrations during an OGTT (2 g/kg) in 24- to 26-week-old HFD-fed wild-type and TBC1D4-S711A mice. Glucose area under the curve (AUC) values during the OGTT are shown in *G*. *I* and *J*: Blood glucose and changes in blood glucose concentrations in anesthetized 25- to 27-week-old HFD-fed wild-type and TBC1D4-S711A mice following retro-orbital injection of vehicle (0.9% saline) with or without insulin (0.75 units/kg). *K* and *L*: In vivo insulin-stimulated glucose uptake in quadriceps muscle and subcutaneous white adipose tissue (ScWAT) from HFD-fed wild-type and TBC1D4-S711A mice. *M–U*: Insulin-stimulated signaling in quadriceps muscle and ScWAT from HFD-fed wild-type and TBC1D4-S711A mice measured at the level of

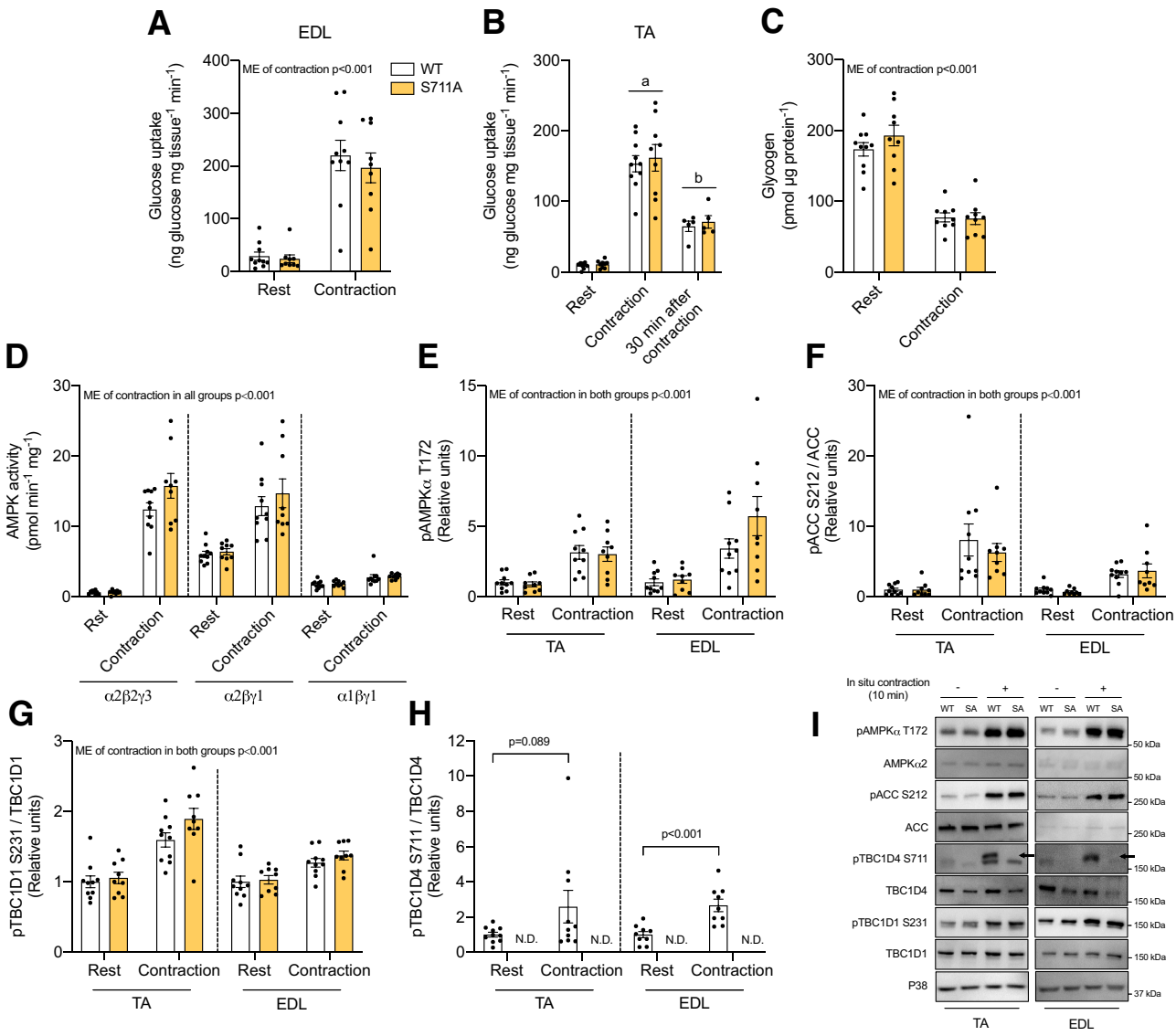

Figure 6—Acute contraction affects glucose uptake, glycogen utilization, and AMPK activation similarly in skeletal muscle from wild-type and TBC1D4-S711A female mice. *A* and *B*: Glucose uptake measured in EDL and tibialis anterior (TA) muscles at rest, during in situ contraction and 30 min after contraction (only TA); a indicates $P < 0.0001$ versus all groups, and b indicates $P < 0.0001$ versus rest group. (*C* and *D*) Glycogen content and heterotrimeric-specific AMPK activity measured in rested and in situ contracted TA muscle. *E–H*: AMPK activation and downstream signaling measured at the level of phosphorylated (p) AMPKα-T172, ACC-S212, TBC1D1-S231, and TBC1D4 S711 in rested and in situ contracted EDL and TA muscle. *I*: Representative immunoblots. Data were analyzed within each muscle type by a Student *t* test (*H*) and a two-way ANOVA without (*B*) and with (*A* and *C–G*) repeated measures. Dots represent individual values, while bar graphs represent means ± SEM (n = 9–10 in all groups except for data on glucose uptake 30 min after contraction, where n = 5). An unspecific band is observed in the TBC1D4-S711 immunoblot. Only the specific TBC1D4 band (upper) has been quantified. Data in *C* were transformed to obtain equal variance prior to statistical testing. ME, main effect; N.D., not detected; WT, wild type; SA, S711A.

contraction are positively associated with insulin-stimulated phosphorylation of TBC1D4-S711 in muscle from wild-type mice but not in muscle from AMPK-deficient mice (26). We have now provided evidence to support that phosphorylation of TBC1D4-S711 is necessary for improving muscle insulin sensitivity after exercise and contraction in female mice. In male TBC1D4-S711A mice, the insulin-sensitizing effect of contraction is also disrupted but not fully abolished. This is in agreement with recent findings by Zheng et al. (47), who reported that adeno-associated virus delivery of a TBC1D4 3P

phosphorylated (p) Akt and TBC1D4. *V*: Representative immunoblots. Data were analyzed by a Student *t* test between genotypes (*B*, *C*, *F*, and *Q*), a two-way repeated ANOVA between genotypes (*D*, *E*, *G*, and *H*), and within treatment (*I*), as well as a two-way ANOVA between genotypes (*J–P* and *R–U*). Dots represent individual values, while bar and line graphs represent means ± SEM (n = 18 in wild-type and n = 14 in TBC1D4-S711A groups in *A–H*, while n = 9 in wild-type and n = 7 in TBC1D4-S711A groups in *I–U*). ME, main effect; N.D., not detected; WT, wild type; SA, S711A.

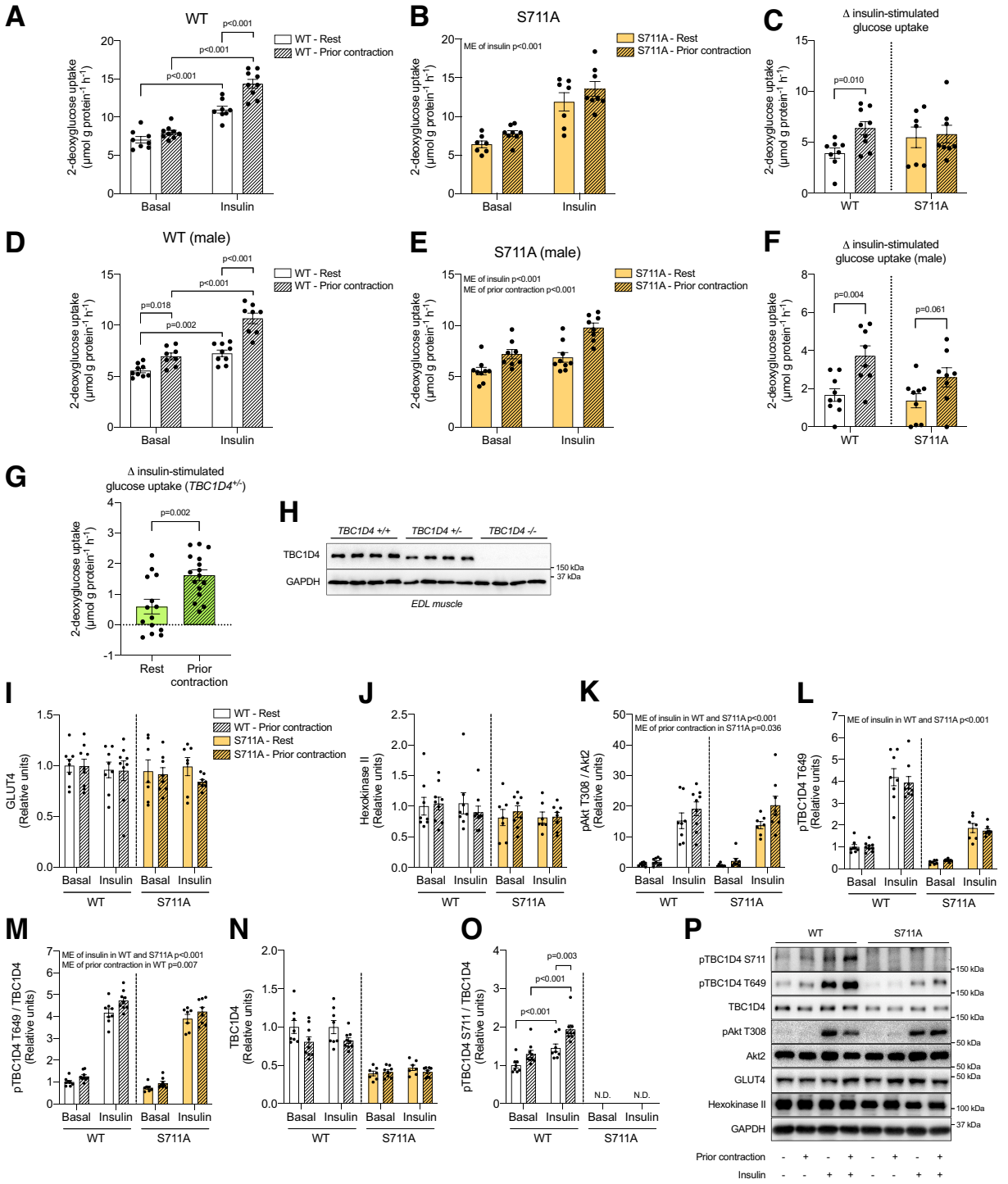

Figure 7—The TBC1D4-S711A mutation disrupts improvements in muscle insulin sensitivity after contraction. *A*, *B*, *D*, and *E*: The 2-deoxyglucose uptake in isolated EDL muscle from wild-type as well as TBC1D4-S711A female (*A* and *B*) and male (*D* and *E*) mice incubated with a submaximal insulin concentration (100 µU/mL) 2 h after rest or in situ contraction. *C* and *F*: Δ insulin-stimulated 2-deoxyglucose uptake calculated from data in *A* and *B* as well as *D* and *E* by subtracting basal 2-deoxyglucose uptake values from values on insulin-stimulated 2-deoxyglucose uptake in paired EDL muscles from each animal. *G* and *H*: Δ insulin-stimulated 2-deoxyglucose uptake (*G*) and representative immunoblot of TBC1D4 protein (*H*) in EDL muscle from heterozygous muscle-specific TBC1D4 KO female mice. *I–O*: TBC1D4, GLUT4, and Hexokinase II protein as well as phosphorylation (p) of Akt-T308, TBC1D4-T649, and TBC1D4-S711 measured in muscles from *A* and *B*. *P*: Representative immunoblots. Data were analyzed by a two-way repeated measures ANOVA within each genotype, except for data in *C*, *F*, and *G* that were analyzed by a Student *t* test within each genotype. Dots represent individual values, while bar graphs represent means ± SEM (n = 7–9 in all groups except for data in *G*, where n = 14–16). ME, main effect; N.D., not detected; WT, wild type.

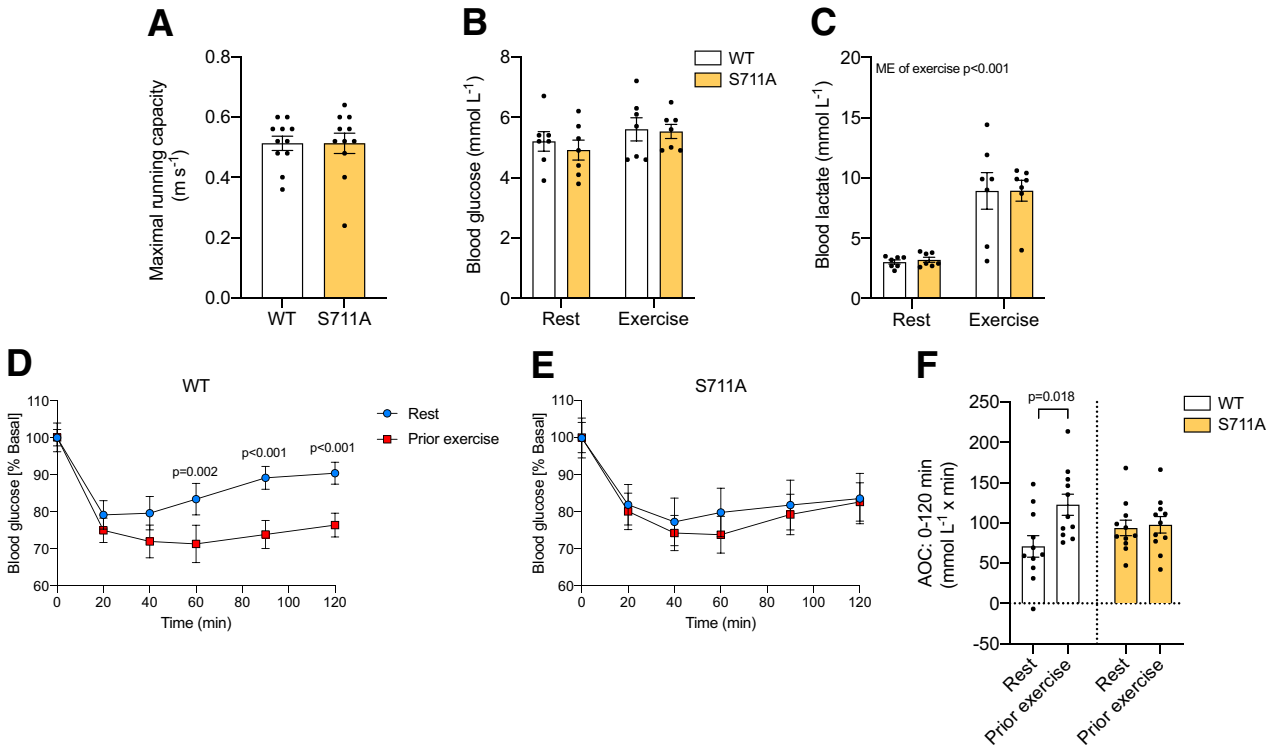

Figure 8—Improvement in whole-body insulin tolerance after a single bout of exercise is impaired in TBC1D4-S711 female mice. *A*: Maximal exercise capacity during treadmill running. *B* and *C*: Blood glucose and lactate concentrations before (rest) and after a maximal running capacity test in wild-type and TBC1D4-S711A mice. *D* and *E*: Blood glucose concentrations (% Basal) from wild-type and TBC1D4-S711A mice during a 120-min submaximal ITT (0.3 units/kg) 1 h after rest or exercise. Absolute blood glucose concentrations at time point 0 min during the ITT in wild-type mice (rest: 4.2 ± 0.1 mmol L^{-1}; prior exercise: 4.2 ± 0.2 mmol L^{-1}; $P = 0.8$) and in TBC1D4-S711A mice (rest: 4.3 ± 0.2 mmol L^{-1}; prior exercise: 4.0 ± 0.2 mmol L^{-1}; $P = 0.2$). *F*: Glucose area over the curve (AOC) values during the ITT. Data were analyzed by a Student *t* test between (*A*) and within (*F*) genotypes as well as a two-way repeated measures ANOVA (*B*–*E*). Dots represent individual values, while bar and line graphs represent means ± SEM (n = 7–11). ME, main effect; WT, wild type.

phosphomutant (S588A, T642A, and S704A) to skeletal muscle of male TBC1D4 KO rats reduced, but did not fully blunt, the insulin-sensitizing effect of exercise. Whether these findings also apply to female rats is currently unknown but may indicate sex-specific differences in TBC1D4-induced augmentation of muscle insulin sensitivity after exercise/contraction.

Lack of TBC1D4 protein in skeletal muscle impairs the ability of exercise and contraction to enhance muscle insulin sensitivity, while restoration of TBC1D4 protein in muscle from TBC1D4 KO animals rescues it (27,47). Although a ∼50% reduction in muscle TBC1D4 protein abundance did not affect basal/resting glucose metabolism in TBC1D4-S711A mice in the current study, such a reduction could potentially have a detrimental effect on the insulin-sensitizing effect of contraction. To illuminate this, we investigated the ability of contraction to improve insulin sensitivity in muscle from heterozygous muscle-specific TBC1D4 KO mice. Notably, prior contraction improved insulin sensitivity in muscle from these mice, demonstrating that the lack of phosphorylated TBC1D4-S711 rather than the reduced TBC1D4 protein abundance is responsible for disrupting improvements in muscle insulin sensitivity after exercise and contraction in TBC1D4-S711A mice.

Exactly how contraction/exercise-induced phosphorylation of TBC1D4-S711 relays improvements in muscle insulin sensitivity remains uncertain, but it is likely related to GLUT4 relocalization to insulin-responsive storage vesicles that augments translocation of GLUT4 to the muscle surface membrane upon subsequent insulin stimulation (11,12). We have recently demonstrated that the exercise-induced phosphorylation of TBC1D4-S711 bound to TBC1D1 is maintained in human skeletal muscle 4 h after a single bout of insulin-sensitizing exercise (46). Because observations from cell-based models support a functional interplay between TBC1D4 and TBC1D1 where phosphorylation of TBC1D4 plays a key role in translating exercise-mimicking stimuli into physical GLUT4-releasing processes that modulate insulin sensitivity for glucose transport (48), it seems reasonable to assume that a disruption of the interplay between TBC1D4 and TBC1D1 in mature skeletal muscle could add further to our understanding of how exercise improves muscle insulin sensitivity.

In conclusion, we show that phosphorylation of TBC1D4-S711 regulates muscle insulin sensitization in response to exercise and contraction. Future studies will have to clarify how phosphorylation of TBC1D4-S711 facilitates enhanced translocation of GLUT4 to the muscle surface membrane

upon insulin stimulation and whether TBC1D4 also acts as a major regulator of insulin sensitivity in human skeletal muscle.

Acknowledgments. The authors would like to thank Betina Bolmgren and Irene Bech Nielsen (Department of Nutrition, Exercise and Sports, Faculty of Science, University of Copenhagen, Denmark) as well as Anja Jokipii-Utzon (Institute of Sports Medicine Copenhagen, Bispebjerg Hospital, Denmark) for their skilled technical assistance. The authors would also like to thank undergraduate student Nicoline Meyer Riisberg (Department of Nutrition, Exercise and Sports, Faculty of Science, University of Copenhagen, Denmark) for her assistance during animal experimentation.

Funding. This work was supported by grants given to J.F.P.W. from the Danish Council for Independent Research Medical Sciences (FSS: 610-00498B) and the Novo Nordisk Foundation (NNF0070370). This work was also supported by a postdoctoral research fellow grant to R.K. from the Danish Diabetes Academy, which is funded by the Novo Nordisk Foundation (NNF17SA0031406), as well as a research grant to R.K. from the European Foundation for the Study of Diabetes/Lilly Young Investigator Research Award Programme. J.T.T. was supported by the Novo Nordisk Foundation Center for Basic Metabolic Research. The Center for Basic Metabolic Research is an independent Research Center at the University of Copenhagen that is partially funded by an unrestricted donation from the Novo Nordisk Foundation (NNF18CC0034900).

Duality of Interest. J.F.P.W. has ongoing collaborations with Pfizer Inc. and Novo Nordisk Inc. unrelated to this work. No other potential conflicts of interest relevant to this article were reported.

Author Contributions. R.K. and J.F.P.W. conceptualized and designed the experiment. R.K., N.O.E., D.F.D., N.R.A., J.B.B., A.G., J.T.T., P.S., and H.P. performed the laboratory analyses. R.K. performed the data analyses. R.K., J.M.K., N.O.E., K.K., D.F.D., and J.K.L. performed the animal experiments. R.K. and J.F.P.W. drafted the manuscript. authors interpreted, reviewed, edited, and approved the manuscript. R.K. and J.F.P.W. are the guarantors of this work and, as such, had full access to all the data in the study and take responsibility for the integrity of the data and the accuracy of the data analysis.

References

1. DeFronzo RA, Tripathy D. Skeletal muscle insulin resistance is the primary defect in type 2 diabetes. Diabetes Care 2009;32(Suppl. 2):S157–S163
2. Richter EA, Mikines KJ, Galbo H, Kiens B. Effect of exercise on insulin action in human skeletal muscle. J Appl Physiol (1985) 1989;66:876–885
3. Wojtaszewski JFP, Hansen BF, Kiens B, Richter EA. Insulin signaling in human skeletal muscle: time course and effect of exercise. Diabetes 1997;46:1775–1781
4. Wojtaszewski JF, Hansen BF, Gade, et al. Insulin signaling and insulin sensitivity after exercise in human skeletal muscle. Diabetes 2000;49:325–331
5. Pehmøller C, Brandt N, Birk JB, et al. Exercise alleviates lipid-induced insulin resistance in human skeletal muscle-signaling interaction at the level of TBC1 domain family member 4. Diabetes 2012;61:2743–2752
6. Cartee GD, Young DA, Sleeper MD, Zierath J, Wallberg-Henriksson H, Holloszy JO. Prolonged increase in insulin-stimulated glucose transport in muscle after exercise. Am J Physiol 1989;256:E494–E499
7. Richter EA, Garetto LP, Goodman MN, Ruderman NB. Muscle glucose metabolism following exercise in the rat: increased sensitivity to insulin. J Clin Invest 1982;69:785–793
8. Castorena CM, Arias EB, Sharma N, Cartee GD. Postexercise improvement in insulin-stimulated glucose uptake occurs concomitant with greater AS160 phosphorylation in muscle from normal and insulin-resistant rats. Diabetes 2014;63:2297–2308
9. Mikines KJ, Sonne B, Farrell PA, Tronier B, Galbo H. Effect of physical exercise on sensitivity and responsiveness to insulin in humans. Am J Physiol 1988;254:E248–E259
10. Sjøberg KA, Frøsig C, Kjøbsted R, et al. Exercise increases human skeletal muscle insulin sensitivity via coordinated increases in microvascular perfusion and molecular signaling. Diabetes 2017;66:1501–1510
11. Hansen PA, Nolte LA, Chen MM, Holloszy JO. Increased GLUT-4 translocation mediates enhanced insulin sensitivity of muscle glucose transport after exercise. J Appl Physiol (1985) 1998;85:1218–1222
12. Knudsen JR, Steenberg DE, Hingst JR, et al. Prior exercise in humans redistributes intramuscular GLUT4 and enhances insulin-stimulated sarcolemmal and endosomal GLUT4 translocation. Mol Metab 2020;39:100998
13. McConell GK, Sjøberg KA, Ceutz F, et al. Insulin-induced membrane permeability to glucose in human muscles at rest and following exercise. J Physiol 2020;598:303–315
14. Fisher JS, Gao J, Han D-H, Holloszy JO, Nolte LA. Activation of AMP kinase enhances sensitivity of muscle glucose transport to insulin. Am J Physiol Endocrinol Metab 2002;282:E18–E23
15. Funai K, Schweitzer GG, Sharma N, Kanzaki M, Cartee GD. Increased AS160 phosphorylation, but not TBC1D1 phosphorylation, with increased postexercise insulin sensitivity in rat skeletal muscle. Am J Physiol Endocrinol Metab 2009;297:E242–E251
16. Needham EJ, Hingst JR, Parker BL, et al. Personalized phosphoproteomics identifies functional signaling. Nat Biotechnol 2022;40:576–584
17. Kramer HF, Witczak CA, Taylor EB, Fujii N, Hirshman MF, Goodyear LJ. AS160 regulates insulin- and contraction-stimulated glucose uptake in mouse skeletal muscle. J Biol Chem 2006;281:31478–31485
18. Treebak JT, Pehmøller C, Kristensen JM, et al. Acute exercise and physiological insulin induce distinct phosphorylation signatures on TBC1D1 and TBC1D4 proteins in human skeletal muscle. J Physiol 2014;592:351–375
19. Chen S, Wasserman DH, MacKintosh C, Sakamoto K. Mice with AS160/TBC1D4-Thr649Ala knockin mutation are glucose intolerant with reduced insulin sensitivity and altered GLUT4 trafficking. Cell Metab 2011;13:68–79
20. Hargett SR, Walker NN, Keller SR. Rab GAPs AS160 and Tbc1d1 play nonredundant roles in the regulation of glucose and energy homeostasis in mice. Am J Physiol Endocrinol Metab 2016;310:E276–E288
21. Treebak JT, Taylor EB, Witczak CA, et al. Identification of a novel phosphorylation site on TBC1D4 regulated by AMP-activated protein kinase in skeletal muscle. Am J Physiol Cell Physiol 2010;298:C377–C385
22. Arias EB, Kim J, Funai K, Cartee GD. Prior exercise increases phosphorylation of Akt substrate of 160 kDa (AS160) in rat skeletal muscle. Am J Physiol Endocrinol Metab 2007;292:E1191–E1200
23. Treebak JT, Frøsig C, Pehmøller C, et al. Potential role of TBC1D4 in enhanced post-exercise insulin action in human skeletal muscle. Diabetologia 2009;52:891–900
24. Funai K, Schweitzer GG, Castorena CM, Kanzaki M, Cartee GD. In vivo exercise followed by in vitro contraction additively elevates subsequent insulin-stimulated glucose transport by rat skeletal muscle. Am J Physiol Endocrinol Metab 2010;298:E999–E1010
25. Schweitzer GG, Arias EB, Cartee GD. Sustained postexercise increases in AS160 Thr642 and Ser588 phosphorylation in skeletal muscle without sustained increases in kinase phosphorylation. J Appl Physiol (1985) 2012;113:1852–1861
26. Kjøbsted R, Munk-Hansen N, Birk JB, et al. Enhanced muscle insulin sensitivity after contraction/exercise is mediated by AMPK. Diabetes 2017;66:598–612
27. Kjøbsted R, Chadt A, Jørgensen NO, et al. TBC1D4 is necessary for enhancing muscle insulin sensitivity in response to AICAR and contraction. Diabetes 2019;68:1756–1766
28. Hingst JR, Bruhn L, Hansen MB, et al. Exercise-induced molecular mechanisms promoting glycogen supercompensation in human skeletal muscle. Mol Metab 2018;16:24–34
29. Steenberg DE, Hingst JR, Birk JB, et al. A single bout of one-legged exercise to local exhaustion decreases insulin action in nonexercised muscle leading to decreased whole-body insulin action. Diabetes 2020;69:578–590
30. Lowry OH, Passonneau JV (Eds.). Typical fluorometric procedures for metabolite assays. In *A Flexible System of Enzymatic Analysis*. Elsevier, 1972, p. 68–92

31. Lundby C, Hellsten Y, Jensen MBF, Munch AS, Pilegaard H. Erythropoietin receptor in human skeletal muscle and the effects of acute and long-term injections with recombinant human erythropoietin on the skeletal muscle. J Appl Physiol (1985) 2008;104:1154–1160
32. Lundby C, Nordsborg N, Kusuhara K, Kristensen KM, Neufer PD, Pilegaard H. Gene expression in human skeletal muscle: alternative normalization method and effect of repeated biopsies. Eur J Appl Physiol 2005;95:351–360
33. Ferré P, Leturque A, Burnol AF, Penicaud L, Girard J. A method to quantify glucose utilization in vivo in skeletal muscle and white adipose tissue of the anaesthetized rat. Biochem J 1985;228:103–110
34. Kjøbsted R, Kido K, Larsen JK, et al. Measurement of insulin-and contraction-stimulated glucose uptake in isolated and incubated mature skeletal muscle from mice. J Vis Exp 2021;171:e61398
35. Barnes BR, Marklund S, Steiler TL, et al. The 5′-AMP-activated protein kinase gamma3 isoform has a key role in carbohydrate and lipid metabolism in glycolytic skeletal muscle. J Biol Chem 2004;279:38441–38447
36. Steinberg GR, O'Neill HM, Dzamko NL, et al. Whole body deletion of AMP-activated protein kinase β2 reduces muscle AMPK activity and exercise capacity. J Biol Chem 2010;285:37198–37209
37. Jørgensen SB, Viollet B, Andreelli F, et al. Knockout of the α_2 but not α_1 5′-AMP-activated protein kinase isoform abolishes 5-aminoimidazole-4-carboxamide-1-β-4-ribofuranosidebut not contraction-induced glucose uptake in skeletal muscle. J Biol Chem 2004;279:1070–1079
38. Kjøbsted R, Roll JLW, Jørgensen NO, et al. AMPK and TBC1D1 regulate muscle glucose uptake after, but not during, exercise and contraction. Diabetes 2019;68:1427–1440
39. Kjøbsted R, Treebak JT, Fentz J, et al. Prior AICAR stimulation increases insulin sensitivity in mouse skeletal muscle in an AMPK-dependent manner. Diabetes 2015;64:2042–2055
40. Jørgensen NO, Kjøbsted R, Larsen MR, et al. Direct small molecule ADaM-site AMPK activators reveal an AMPKγ3-independent mechanism for blood glucose lowering. Mol Metab 2021;51:101259
41. Basse AL, Dalbram E, Larsson L, Gerhart-Hines Z, Zierath JR, Treebak JT. Skeletal muscle insulin sensitivity show circadian rhythmicity which is independent of exercise training status. Front Physiol 2018;9:1198
42. Yang X, Chen Q, Ouyang Q, et al. Tissue-specific splicing and dietary interaction of a mutant *As160* allele determine muscle metabolic fitness in rodents. Diabetes 2021;70:1826–1842
43. Cooper TA, Mattox W. The regulation of splice-site selection, and its role in human disease. Am J Hum Genet 1997;61:259–266
44. Duan J, Wainwright MS, Comeron JM, et al. Synonymous mutations in the human dopamine receptor D2 (DRD2) affect mRNA stability and synthesis of the receptor. Hum Mol Genet 2003;12:205–216
45. Moltke I, Grarup N, Jørgensen ME, et al. A common Greenlandic TBC1D4 variant confers muscle insulin resistance and type 2 diabetes. Nature 2014; 512:190–193
46. Larsen JK, Larsen MR, Birk JB, et al. Illumination of the endogenous insulin-regulated TBC1D4 interactome in human skeletal muscle. Diabetes 2022;71:906–920
47. Zheng A, Arias EB, Wang H, et al. Exercise-induced improvement in insulin-stimulated glucose uptake by rat skeletal muscle is absent in male AS160-knockout rats, partially restored by muscle expression of phosphomutated AS160, and fully restored by muscle expression of wild-type AS160. Diabetes 2022;71:219–232
48. Hatakeyama H, Morino T, Ishii T, Kanzaki M. Cooperative actions of Tbc1d1 and AS160/Tbc1d4 in GLUT4-trafficking activities. J Biol Chem 2019;294: 1161–1172